Free Pyrene Probes in Gel and Fluid Membranes: Perspective through Atomistic Simulations

ARTICLE *in* THE JOURNAL OF PHYSICAL CHEMISTRY B · MAY 2007

Impact Factor: 3.3 · DOI: 10.1021/jp065956w · Source: PubMed

5 AUTHORS, INCLUDING:

Pavla Capkova
Jan Evangelista Purkyně University
138 PUBLICATIONS **1,179** CITATIONS
SEE PROFILE

Jaromir Plasek
Charles University in Prague
61 PUBLICATIONS **644** CITATIONS
SEE PROFILE

Ilpo Vattulainen
Tampere University of Technology
283 PUBLICATIONS **7,881** CITATIONS
SEE PROFILE

Free Pyrene Probes in Gel and Fluid Membranes: Perspective through Atomistic Simulations

Jana Čurdová

Department of Chemical Physics and Optics, Faculty of Mathematics and Physics, Charles University, Ke Karlovu 3, Prague 2, CZ-12116, Czech Republic

Pavla Čapková

Department of Chemical Physics and Optics, Faculty of Mathematics and Physics, Charles University, Ke Karlovu 3, Prague 2, CZ-12116, Czech Republic

Jaromír Plášek

Institute of Physics, Charles University, Ke Karlovu 5, Prague 2, CZ-12116, Czech Republic

Jarmila Repáková

Laboratory of Physics and Helsinki Institute of Physics, Helsinki University of Technology, P.O. Box 1100, FI-02015 HUT, Finland

Ilpo Vattulainen*

Institute of Physics, Tampere University of Technology, P.O. Box 692, FI-33101 Tampere, Finland, Laboratory of Physics and Helsinki Institute of Physics, Helsinki University of Technology, P.O. Box 1100, FI-02015 HUT, Finland, and MEMPHYS−Center for Biomembrane Physics, University of Southern Denmark, Odense, Finland

Received: September 12, 2006; In Final Form: February 8, 2007

We consider the properties of free pyrene probes inside gel- and fluidlike phospholipid membranes and unravel their influence on membrane properties. For this purpose, we employ atomic-scale molecular dynamics simulations at several temperatures for varying pyrene concentrations. Molecular dynamics simulations show that free pyrene molecules prefer to be located in the hydrophobic acyl chain region close to the glycerol group of lipid molecules. Their orientation is shown to depend on the phase of the membrane. In the fluid phase, pyrenes favor orientations where they are standing upright in parallel to the membrane normal, while, in the gel phase, the orientation is affected by the tilt of lipid acyl chains. Pyrenes are found to locally perturb membrane structure, while the nature of perturbations in the gel and fluid phases is completely different. In the gel phase, pyrenes break the local packing of lipids and decrease the ordering of lipid acyl chains around them, while, in the fluid phase, pyrenes increase the ordering of nearby acyl chains, thus having an opposite effect. Interestingly, this proposes a similarity to effects induced by cholesterol on structural membrane properties above and below the gel−fluid transition temperature. Further studies express a view that the orientational ordering of pyrene is not a particularly good measure of the acyl chain ordering of lipids. While pyrene ordering provides the correct qualitative behavior of acyl chain ordering in the fluid phase, its capability to predict the correct temperature dependence is limited.

I. Introduction

Biological membranes[1] are essentially lipid bilayers in which many biological molecules such as integral proteins and lipid-linked glyco-moieties are embedded. The biological relevance of membranes is captured by the lipid raft model[2] which together with recent findings[3,4] has shown that a variety of cellular processes such as signal transduction and protein sorting are facilitated or even governed by cellular membranes. Recently, membranes have also been used more and more in biotechnological applications such as drug delivery.[5,6]

Resolving the properties of soft-matter systems, which are driven by weak interactions of the order of thermal energy, is a great challenge. As for lipid membranes, one of the commonly used experimental means to probe their structure and dynamics is fluorescence spectroscopy together with related imaging techniques.[7,8] These methods are based on the use of fluorescent probes[9,10] such as pyrene, diphenylhexatriene, and prodan, which either are linked to other molecules via covalent bonds or diffuse freely within a membrane. Hydrophobic probes are an obvious tool to gauge structures in the hydrocarbon region of a membrane, while polar and charged probes provide one with an opportunity to explore the polar head group region close to the membrane−water interface. Consequently, fluorescent probes are commonly employed to elucidate a great variety of membrane processes such as domain formation,[11] diffusion of lipids,[12] membrane fluidity,[9,13,14] and hence also phase behavior.

* Author to whom correspondence should be addressed. E-mail: Ilpo.Vattulainen@csc.fi.

10.1021/jp065956w CCC: $37.00
Published on Web 03/20/2007

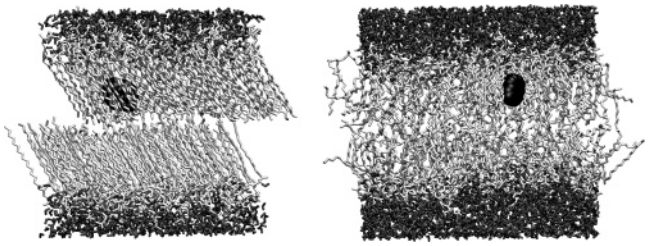

Figure 1. Snapshots of simulated DPPC bilayers together with pyrene molecules inside the membrane in the gel (left) and fluid (right) phases.

However, since probes are not an integral native component of membranes, it is inevitable that they perturb membrane structures and dynamics to some extent. Experimentally, it has been observed that probes may affect, for example, the main phase transition temperature of a given membrane system[9,15−17] and the ordering of lipid acyl chains.[18] However, since the molar concentrations of probes used in fluorescent studies are often very small, of the order of 0.1−1 mol %, resolving the magnitude of probe-induced perturbations is very difficult through experiments whose results are averaged over the whole system. To shed more light on the issue, atomistic simulations have recently been employed to characterize the nature and significance of probe-induced perturbations,[18,19] and to unravel the location and other structural and dynamical properties of probes.[14,20] The impact of simulation studies has turned out to be significant, as they have provided one with deep insight into the effects of probes with an atomistic level of detail not within reach by experiments.

In the present work, we assess the significance of membrane perturbations due to free pyrene. Pyrene[21] is a polycyclic aromatic hydrocarbon, exhibiting toxic, mutagenic, and carcinogenic properties dangerous for human health.[20] Pyrene is a rigid, planar molecule with zero total charge. Due to its hydrophobic nature, this molecule diffuses passively into a cell membrane and accumulates in the acyl chain region of the lipid bilayer; see below. Pyrene probes (see Figure 2) are widely used in studies of the structure and dynamic properties of biomembranes and cells,[22] and they can be used for fluorescent labeling of different phase states of membranes.[20,23] One of the most important properties of pyrene is its ability to form excimers and exciplexes which yield a structureless emission band within the visible range.[7,22] The pyrene excimer (excited-state dimer) formation is commonly exploited for assaying membrane fusion.[24]

The location of pyrene and its properties within a membrane have been characterized experimentally in a number of studies.[12,20,22,24−26] Fluorescence decay measurements of pyrene in fluid dipalmitoylphosphatidylcholine (DPPC) vesicles at different temperatures and concentrations have provided information about the excimer lifetimes, which have turned out to be on a scale of nanoseconds.[22,24] References 22 and 24 also considered the lateral diffusion of pyrene and have later been complemented by fluorescence self-quenching measurements in dimyristoylphosphatidylcholine (DMPC) vesicles.[12] When it comes to pyrene-induced membrane perturbations, differential scanning calorimetry applied to DMPC vesicles has shown that pyrene causes a detectable reduction of the main phase transition temperature, T_M.[25] As for simulations, there is only the recent work by Hoff et al., who combined simulations with NMR experiments to consider the case of free pyrene in a fluid palmitoyloleoylphosphatidylcholine (POPC) bilayer.[20] The study of Hoff et al. proposed that free pyrene probes prefer to be positioned in the hydrophobic part of a membrane near the head group region, with the long axis of the probe being approximately in parallel to the bilayer normal.[20] Other experimental studies based on fluorescent quenching support this view.[26]

The objective of this work is twofold. First, we consider the properties of free pyrene probes in a membrane, focusing on the orientation and distribution of pyrene in the membrane. Second, we address the influence of perturbations induced by pyrene on membrane structure and dynamics. Both studies are carried out for various pyrene concentrations at several temperatures, considering the cases of both the fluid and gel phases. Previously, the gel phase properties of pure lipid bilayers were elucidated only in a few computational studies.[27−31] Further, to our knowledge, there are no previous computational studies of probe-induced effects in the gel phase.

We have found that pyrene molecules prefer to be located in the hydrophobic acyl chain region of a DPPC membrane under the glycerol group. Pyrenes are mainly oriented in a manner where their longest principal axis is in parallel with the bilayer normal, though in the gel phase the orientational distribution is broader due to the tilt of lipid acyl chains with respect to the membrane normal. Although pyrene is a rigid and quite large molecule, its effect on membrane properties turns out to be rather modest. Only the lipids neighboring pyrene moieties are significantly affected by pyrene, with the correlation length of perturbations in the bilayer plane being about two molecular diameters. What is remarkable, though, is the different action of pyrene in the gel and fluid phases. In the gel phase, pyrene locally breaks the order of the solidlike gel phase, decreasing the conformational ordering of neighboring lipid acyl chains, while, in the fluid phase, pyrenes locally increase the conformational ordering of lipid chains. In this respect, pyrene seems to act in a similar fashion as cholesterol in model membranes.

II. Model and Simulation Details

Our purpose is to elucidate the properties of pyrene probes and their influence on a lipid bilayer. For this purpose, we simulated a system comprised of pyrene molecules embedded in a one-component dipalmitoylphosphatidylcholine (DPPC) bilayer surrounded by water (see Figure 1). Simulations were conducted at various temperatures in the fluid (liquid-disordered) and gel phases, and at several pyrene concentrations; see below.

The main phase transition temperature, T_M, of a one-component DPPC bilayer is about 314 K,[1] which differentiates the gel phase ($T < T_M$) from the fluid phase ($T > T_M$). Here, we considered several temperatures around T_M: 273, 293, 325, and 350 K. The simulation in the gel phase was carried out at 273 K. In this case, we built a lipid bilayer composed of 120 DPPC and 1429 water molecules (see Figure 1), which corresponds to a fully hydrated lipid bilayer in the gel phase.[32,33] The initial configuration of the DPPC bilayer system used in this case was based on a previous gel phase DPPC simulation (after a simulation[34] of 50 ns), which in turn was started from a fully ordered gel phase DPPC bilayer. For systems at higher temperatures (293, 325, and 350 K), the simulations were started from a fluid initial configuration, with the starting structure corresponding to the final structure of run E[35] available at http://moose.bio.ucalgary.ca/index.php?page=Downloads. This model of 128 DPPCs was hydrated by 3655 water molecules.

The model at 293 K was started from a fluidlike initial state, since our purpose was to consider the freezing of the bilayer system. However, as it becomes apparent below, this system did not achieve the true gel phase but instead showed a partly ordered gel-like bilayer with remnants of the fluid phase. Hence,

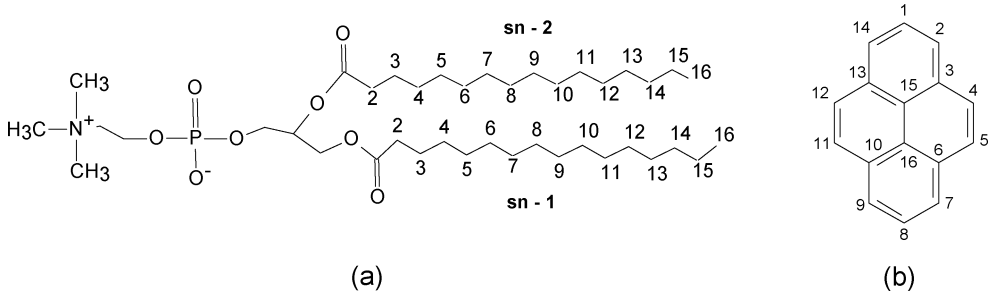

Figure 2. Structures of the (a) DPPC and (b) pyrene molecules used in this study.

TABLE 1: Partial Charges of Atoms in Pyrene Derived from ab Initio Calculations with the Hartree−Fock Method and the 6-31G Basis Set[a]

number	partial charge	number	partial charge
1	0.092	9	−0.157
2	−0.157	10	0.224
3	0.224	11	−0.082
4	−0.082	12	−0.082
5	−0.082	13	0.224
6	0.224	14	−0.157
7	−0.157	15	−0.062
8	0.092	16	−0.062

[a] Numbering of atoms corresponds to Figure 2b.

TABLE 2: Results for the Average Area per Lipid in DPPC Bilayers at Different Temperatures and Pyrene Concentrations

temperature (K)	pyrene/lipid ratio	$\langle A \rangle$ (nm^2)
273	0:120	0.515 ± 0.003
273	1:120	0.514 ± 0.010
273	3:120	0.527 ± 0.008
325	0:128	0.695 ± 0.006
325	1:128	0.683 ± 0.005
325	3:128	0.685 ± 0.004
350	0:128	0.719 ± 0.005
350	1:128	0.717 ± 0.006
350	3:128	0.720 ± 0.005

we do not discuss these results in great detail but instead only summarize their main features at the end of this article.

The free pyrene probes (see Figure 2) were built and manually inserted into the hydrocarbon region of the DPPC bilayers using Cerius^2.[36] The probes were inserted in a random manner, meaning that the pyrene positions in the bilayer plane, their locations in the hydrophobic acyl chain region, as well as their orientations were chosen randomly. For systems with three probes, their distribution in the two leaflets was chosen such that all three probes were not in the same monolayer. The concentrations of pyrene in the membranes were chosen to reflect experimental conditions, where the pyrene/DPPC molar ratio ranges from 1:3000 to 1:50.[12,24] Our molar concentrations were 0:128, 1:128, and 3:128 in the fluid phase and 0:120, 1:120, and 3:120 in the gel phase. At the highest concentrations, the probes were randomly placed into the membrane; this concentration corresponds to experimental conditions for excimer formation.[24]

We employed a united-atom description for DPPC and pyrene molecules, that is, −CH, −CH_2, and −CH_3 groups were treated as single united interaction centers.[35] The parameters for bonded and nonbonded interactions were taken from a study of a pure DPPC membrane[37] available at http://moose.bio.ucalgary.ca/files/dppc.itp. The parameters for pyrene were chosen through a combination of similar atom types in a model of DPPC.[37] The partial charge distribution on each atom of pyrene was derived from ab initio quantum-mechanical calculations using[38] Gaussian 97 with the Hartree−Fock method and the 6-31G basis set; see Table 1. For water molecules, we used the single point charge (SPC) model.[39]

Short-range interactions were cut off at 0.9 nm. A similar value has been used in a recent study of diphenylhexatriene, which is also a commonly employed fluorescent probe.[14] Another commonly used truncation distance for short-range interactions is 1.0 nm, which leads to a slightly smaller area per lipid due to the attractive tail of the interactions in question. The nature of the results concerning pyrene-induced perturbations is not affected by the precise value of the truncation distance, though. This is discussed and confirmed in section III.G. As for long-range electrostatic interactions, the truncation has been shown to lead to somewhat artificial membrane structures;[40,41] thus, we employed the particle-mesh Ewald technique[42] which has been shown to do well in membrane simulations.[40,41,43]

All simulations were carried out by the GROMACS software package[44] in the *NpT* ensemble. The temperature and pressure of the simulated system were controlled by the Berendsen algorithm.[39] The coupling constants of temperature and pressure were 0.1 and 1.0 ps, respectively. The lengths of all bonds were constrained with the LINCS algorithm.[45] Subsequently we applied periodic boundary conditions in all three dimensions. The simulations were performed over a time scale of 20 and 50 ns in the fluid and gel phases, in respective order. The time step in both cases was 2.0 fs. The force field employed in this work has been previously used with minor modifications in a number of studies of membrane properties, such as ion leakage across membranes,[46] the distribution and shape of free volume pockets inside a membrane,[47,48] and the influence of sterols on membranes.[49,50]

III. Results and Discussion

A. Area per Lipid. The area per lipid in the bilayer plane provides a reliable means to control equilibration of the lipid bilayer system, as it affects various membrane properties such as lateral diffusion and ordering of hydrocarbon chains. Therefore, we calculated the area per lipid, $A(t)$, for each frame of the simulations at time t by dividing the area of the membrane by the number of DPPC molecules in one leaflet.

Results for $A(t)$ at different temperatures indicated that the systems equilibrated in 10 ns (data not shown); thus, we discarded the first 10 ns of the simulations and used the remaining period for analysis. Table 2 summarizes the data and shows the dependence of the average area per lipid, $\langle A \rangle$, on temperature. We find that $\langle A \rangle$ increases with temperature. The lowest value of 0.51 nm^2 found in the gel phase at 273 K for a pure DPPC bilayer is in agreement with the experimental result[32] of 0.47 nm^2 and results from the (almost) all-trans conformations of acyl chains together with the tilted orientation of lipids with respect to the membrane normal, which lead to largely

hexagonal packing of the lipids in the bilayer plane. At higher temperatures, the hydrocarbon chains are more disordered, leading to increasing area per lipid. The average value found at 325 K, $\langle A \rangle = 0.69$ nm^2, is in reasonable agreement with experiments, which have yielded a value of 0.64 nm^2.[51] The slight systematic difference observed between simulations and experiments for $\langle A \rangle$ is likely due to the cutoff distance of 0.9 nm used in this study for van der Waals interactions. The same DPPC model with a cutoff of 1.0 nm has given the area per lipid of 0.64 nm^2 at 323 K.[40,49]

Table 2 shows that the effect of pyrene on the average area per lipid is very small. To our knowledge, experimental data for the effect of pyrene on lipid bilayers is not available for comparison. Below T_M, the simulation results indicate that pyrene slightly increases $\langle A \rangle$, while, above T_M, the effect is of the opposite nature. The below results for S_{CD} order parameters support this view; see the next section. However, since the results for $\langle A \rangle$ have been determined as an average over all lipids in a bilayer and the molar concentration of pyrene is very small, the possible effects of pyrene on the average area per lipid are expected to be minor, too. We discuss this matter in more detail below, where we gauge the influence of pyrene probes on their local surrounding.

B. Order Parameter Profiles. Several membrane probes are used to gauge membrane fluidity, which is related to the packing and ordering of lipid acyl chains. Here, we therefore investigate the influence of pyrene on the bilayer structure through the deuterium order parameter, $|S_{CD}|$, which characterizes the average conformational ordering of lipid hydrocarbon chains and is readily measured by NMR.[52] In our simulations, the order parameter is characterized via the tensor

$$S_{ij} = \frac{1}{2}\langle 3 \cos \theta_i \cos \theta_j - \delta_{ij} \rangle \quad (1)$$

where $i, j = x, y, z$ and θ_i is the angle between the molecular i-axis and the bilayer normal.[53] In our simulations, z is along the $C_{n-1}-C_{n+1}$ direction, the carbons C_{n-1}, C_n, and C_{n+1} span the yz-plane, and x is perpendicular to the yz-plane. As discussed in refs 53 and 54, the experimentally observed S_{CD} value is then related to the tensor components by

$$-S_{CD} = \frac{2}{3}S_{xx} + \frac{1}{3}S_{yy} \quad (2)$$

If the rotation around the molecular z-axis is isotropic, then the above relation reduces to[53]

$$S_{CD} = S_{zz}/2 \quad (3)$$

This is the case in the fluid phase, where simulated time scales are long enough and the rotations around the molecular z-axis are isotropic. In the gel phase, however, this is not as obvious due to insufficient sampling. For that reason, we employed eq 2 in the gel phase (though the results given by eq 3 were almost similar) and eq 3 in the fluid phase (though in the fluid case eq 2 would also be a proper choice). We have computed $|S_{CD}|$ for all carbon atoms in both chains (*sn*-1 and *sn*-2) for all concentrations of pyrene.

The order parameter profiles are depicted in Figure 3. Let us first concentrate on the pure DPPC system shown at the top row of Figure 3 (lines without symbols). As we can see, the values of S_{CD} decrease with increasing temperature. Above the main phase transition temperature, T_M, they additionally decrease for increasing distance from the polar head group region, with an exception of the carbons closest to the glycerol group. The S_{CD} profiles for temperatures 325 and 350 K above T_M are qualitatively similar. The reduction of order along the chains as one approaches the membrane center reflects increasing flexibility and accelerated dynamics in the chains. Below T_M at 273 K, the behavior of S_{CD} is somewhat different. In this case in the gel phase, the S_{CD} profile for the first 12 carbons is almost flat. This illustrates the ordered structure of the membrane and in particular the almost optimal all-trans nature of lipid acyl chains as they are tightly packed in a membrane.

There is reason to point out that here we have calculated the order parameter with respect to the membrane normal. This implies that the maximum value of S_{CD} is then about 0.5, which happens if a chain is in an all-trans configuration and standing upright along the membrane normal direction. In the fluid phase, this implies that the order parameters shown in Figure 3 are about one-third of their maximal values, confirming that we are indeed dealing with a fluid phase. In the gel phase, however, the acyl chains are tilted with respect to the membrane normal. If this tilt of about 33° (see discussion below and Figure 1) were accounted for, the maximal value of S_{CD} in the gel phase would be about 0.28. As the plateau value of S_{CD} in the gel phase for a pure DPPC bilayer in Figure 3 (see the top row) is 0.24−0.25, we find that there is substantial conformational order below T_M.

Our results for the pure DPPC system are in good agreement with previous simulations and experiments. At temperatures above the main phase transition temperature, the results are in agreement with experimental data obtained from NMR spectroscopy[55,56] and previous simulations.[18,20,40] The gel phase results are also in close agreement with previous simulations at 250 K by Sum et al.[31]

Incorporating pyrenes into membranes gives rise to perturbations; see again the top row in Figure 3. Lines without symbols indicate profiles for the pure DPPC system, while the lines with symbols correspond to systems with three pyrenes embedded in a bilayer. Below T_M, the effect of pyrenes is rather weak; however, what we can observe is a slight change in the order parameter values. We discuss this issue in more detail below. At temperatures above T_M, it seems that pyrenes increase the average lipid chain ordering. The effect is minor but evident. In any case, some care should be taken when conclusions are being drawn, since the scatter between the results for the *sn*-1 and *sn*-2 chains indicates that the differences in these profiles are rather minor. This is largely due to the fact that the molar concentration of pyrenes is small; hence, the perturbations in the profiles *averaged over all lipids in a bilayer* are also expected to be minor. For the same reason, differences of this size are very difficult to gauge through experiments by NMR.[18]

To consider the influence of pyrenes in more detail, we next gauge their *local effect* exerted on those lipids that are neighbors to the pyrene. For this purpose, we define D as the distance from the center of mass (CM) of a tagged DPPC to the center of mass of the nearest pyrene. Calculations were carried out in the same way as in the previous study for diphenylhexatriene.[18] Since the results for pyrene/lipid ratios of 1:128 and 3:128 in the fluid phase (and 1:120 vs 3:120 in the gel phase) were very similar, we present $|S_{CD}|$ profiles only for the largest pyrene concentration 3:128. The order parameter profiles for the *sn*-1 and *sn*-2 chains are shown on the last four rows in Figure 3.

First, generally speaking, one can conclude that pyrene probes affect only those DPPCs that are their nearest or next nearest neighbors. This local perturbative effect is easy to understand in the fluid phase, where the lack of translational symmetry in the bilayer plane weakens the possible range of perturbations.

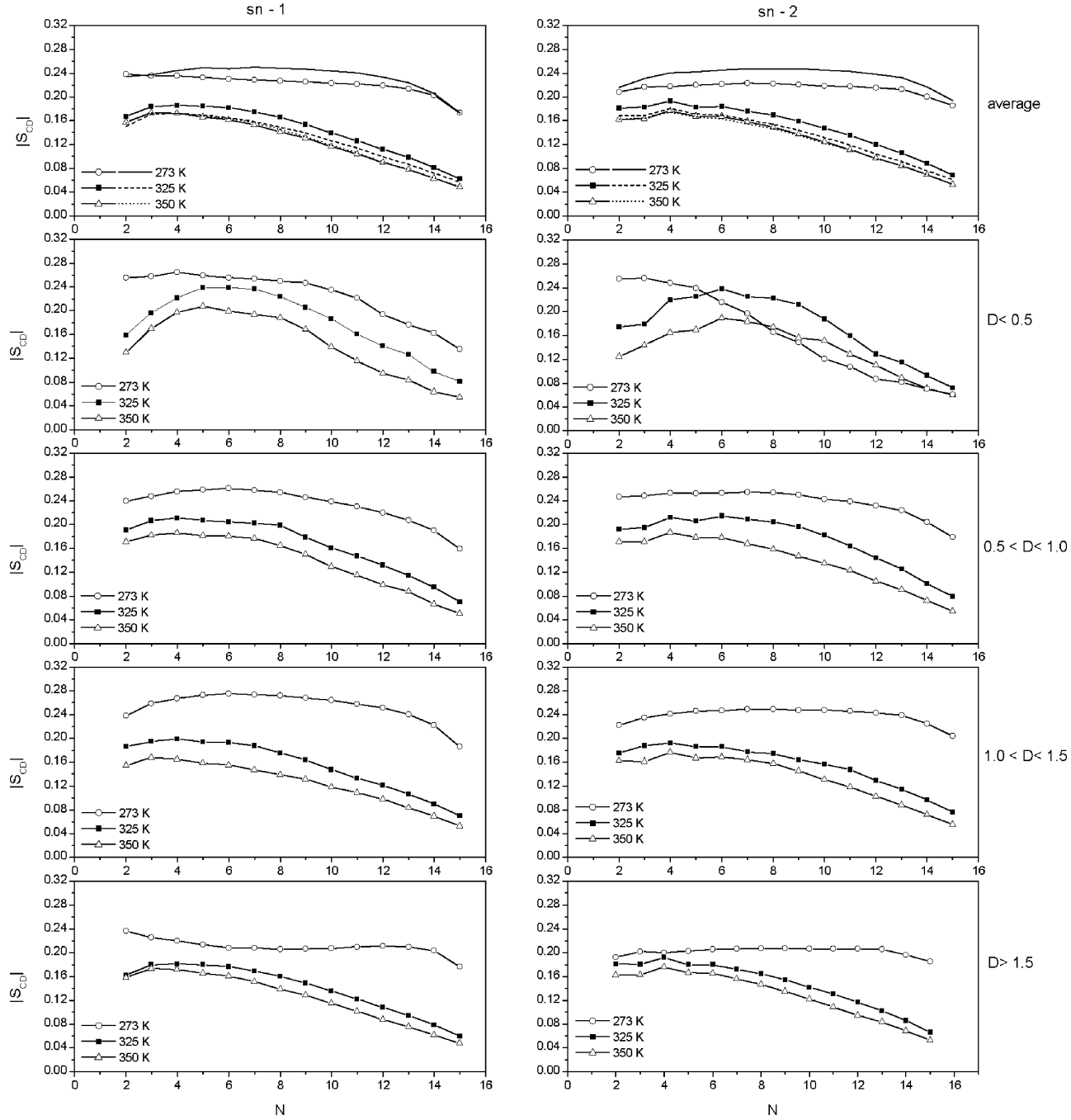

Figure 3. $|S_{CD}|$ order parameter profiles for *sn*-1 (left) and *sn*-2 (right) chains of DPPCs at several temperatures. The results shown here are for the pure DPPC system (lines without symbols) and for the case where three pyrenes are embedded in the DPPC bilayer (lines with symbols). *N* denotes the position of the carbon atom in the acyl chain (see Figure 2), with small numbers corresponding to carbons close to the glycerol group. From top to bottom, the first row shows the results for the order parameters averaged over all lipids in a system, while the last four rows show results for the lipids close to pyrene. Here, we have defined *D* as the distance from the center of mass of a tagged DPPC to the center of mass of the nearest pyrene. As for error estimates, they are very small for the profiles averaged over all lipids and for $D > 1.5$ nm and largest for $D < 0.5$ nm (about 10%).

Previous studies of diphenylhexatriene have yielded a similar conclusion[18] in the fluid phase. The gel phase case is less obvious. There, one might have expected perturbations to have a longer range, since the gel phase is characterized by quasi-long-range translational ordering in membrane plane. However, the "defects" generated by pyrene probes seem to perturb only the packing around them, and no long-range effects are observed.

A more detailed comparison of the plots in Figure 3 indicates that the influence of pyrene on the gel and fluid phase structures is actually very different. Let us first focus on the fluid phase. We find that the profiles for $D < 0.5$ nm differ substantially from the average case: the acyl chains of the DPPCs next to pyrene molecules are considerably more ordered than the lipids on average. This effect is most prominent for acyl chain segments close to the head group region (carbons ~2−8). This region matches the one where pyrene probes are mainly located; see the next section. For larger distances ($0.5 \text{ nm} < D < 1.0$ nm), one can find the same effect for intermediate carbons 2−8, but for $D > 1.0$ nm, the additional ordering effect of pyrene is essentially negligible.

The influence of pyrenes on the gel phase structure is more

complicated, though. Figure 3 at 273 K shows that the largest values of $|S_{CD}|$ for various values of D are about 0.26−0.28. These values are larger than the average value of about 0.22 computed over the whole system and also comparable to the optimal value of 0.28 in the gel phase for an acyl chain tilted by 33°. However, as discussed below, we found that the fraction of gauche states increased in the vicinity of pyrene; thus, the lipids neighboring the probe could not be in a fully ordered (all-trans) conformational state. Hence, the only way to interpret this result is that the acyl chains closest to a pyrene are tilted less than the chains far from the probe. It turns out that this is indeed the case. For the gel phase simulation with three pyrenes at 273 K, we computed the tilt angle, ϕ, between the membrane normal and the vector from the terminal carbon C16 to the carbon C2 (see Figure 2). For the *sn*-2 chain, for example, we found $\phi = 25°$ for $D < 0.5$ nm, 29° for 0.5 nm $< D <$ 1.0 nm, 33° for 1.0 nm $< D <$ 1.5 nm, and 34° for $D >$ 1.5 nm. On average, the tilt angle was 33° (for both the *sn*-1 and *sn*-2 chains), in agreement with experiments which have yielded 32°.[33,57] The smaller tilt of acyl chains close to pyrene is in favor of reduced conformational order due to the probe. Results for the average trans/gauche fractions along the acyl chains support this conclusion: we found for the same system that the average trans fraction was 0.857 ± 0.052 for chains close to pyrene, and 0.889 ± 0.007 for a case where one averaged over all the chains in the system. To further quantify the above findings, we computed the S_{CD} profiles separately for each leaflet such that the calculation was carried out with respect to the average lipid tilt direction in a given monolayer (instead of the membrane normal). In this manner, the maximum of the order parameter in the gel phase is 0.5. The results (not shown) were consistent with the above view.

In conclusion, the above analysis supports a view that in the fluid phase pyrenes locally increase the conformational ordering of lipid acyl chains that are in their vicinity. In the gel phase, however, free pyrenes instead decrease the ordering of those hydrocarbon chains that are closest to the pyrene ($D <$ 1.0 nm). For comparison, it is interesting to realize a coupling to the action of cholesterol on (saturated) lipid acyl chains. It is well-known for two-component PC−cholesterol membranes that in the fluid phase cholesterol locally increases the conformational order around it, while in the gel phase it disturbs the packing of lipids and locally increases the disorder. As both cholesterol and pyrene are rigid molecules and standing upright along the membrane normal, this similarity seems to be justified and based, at least in part, on steric constraints imposed by their rigid structure.

C. Density Profiles, Pyrene Location, and Its Orientation. To elucidate the positions of pyrene probes and different groups in lipids, we calculated the mass and electron density profiles across the membrane. The density profiles in the membrane normal (z) direction were computed with respect to the instantaneous CM position of the bilayer, and the final density profiles were averaged over the two leaflets. The mass density profiles computed at different temperatures and concentrations of pyrenes and for different components across the bilayer are shown in Figure 4.

In experiments, one usually measures the electron density profile, which provides one with an estimate of membrane thickness defined as the distance between the two electron rich main peaks (often associated with contributions due to phosphor) in the opposing leaflets, d_{PP}. A similar calculation for electron density profiles based on our simulations yielded the membrane thicknesses shown in Table 3.

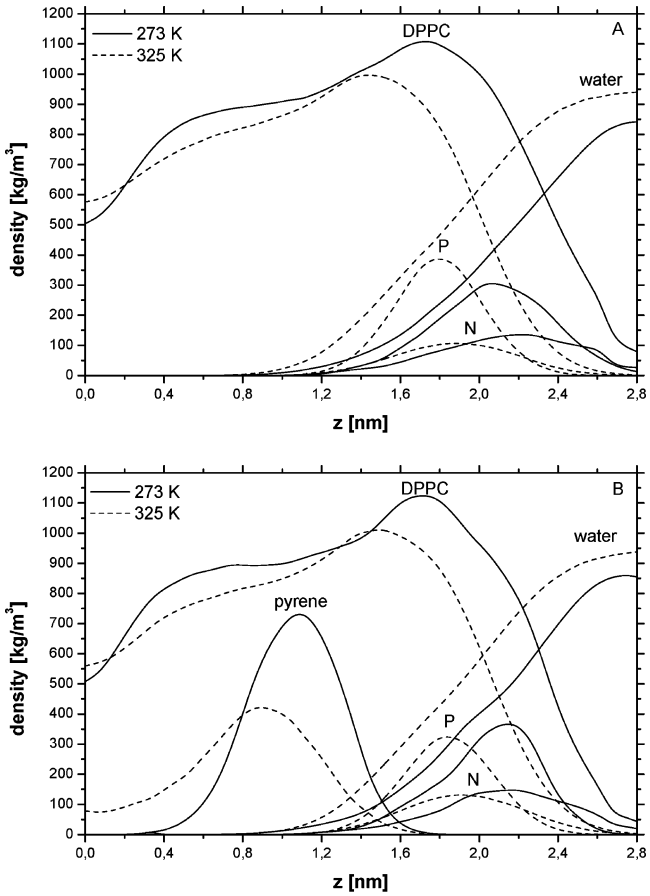

Figure 4. Mass density profiles as a function of distance z from the bilayer center: (A) a pure DPPC bilayer; (B) a DPPC membrane with three pyrenes. For clarity's sake, we only show results at two temperatures, 273 and 325 K, to illustrate the gel and liquid-disordered phases, respectively. Also, for clarity, the mass density profiles of pyrene, nitrogen, and phosphor atoms have been multiplied by a factor of 30, 2.5, and 3.0, in respective order.

TABLE 3: Membrane Thickness at Different Temperatures and for Several Pyrene Concentrations[a]

temperature (K)	pyrene/lipid ratio	d_{PP} (nm)
273	0:120	4.08
273	1:120	3.92
273	3:120	3.76
325	0:128	3.38
325	1:128	3.46
325	3:128	3.50
350	0:128	3.34
350	1:128	3.37
350	3:128	3.40

[a] The thickness is defined as the distance between the main peaks (due to phosphor rich groups) in the opposing leaflets of the total electron density profile.

Several interesting aspects emerge. For increasing temperature, we find membrane thickness to decrease. This behavior is well-known and reflects the disordering of the membrane at higher temperatures. Next, there is a major change in membrane thickness as one crosses the gel−fluid transition temperature. This also is associated with the change in the conformational ordering of lipid acyl chains but also with the disappearance of the quasi-long-range translational order typical for the gel phase but lacking from the fluid phase membrane. Hence, as one crosses the gel−fluid transition, the increase of the average area per lipid is partly compensated by a reduction in membrane

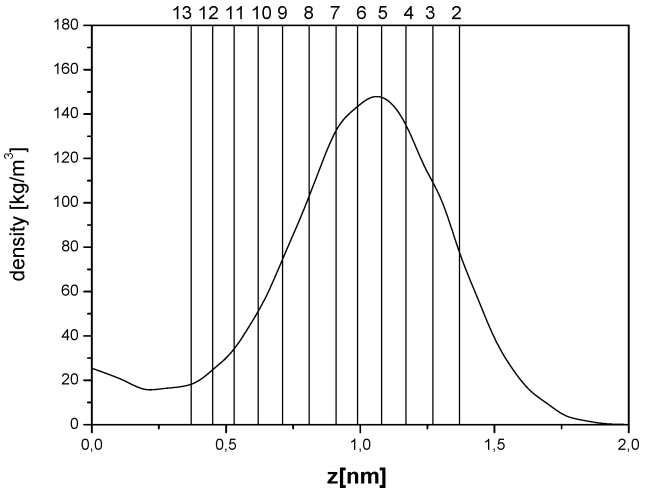

Figure 5. Mass density profiles of a single pyrene as a function of distance from the bilayer center at 325 K. Also shown are the average positions of carbon atoms of lipid molecules in the *sn*-1 chain.

thickness, such that the volume taken by the membrane does not change significantly.

The effect of pyrene on membrane thickness clearly depends on the phase one is looking for. In the gel phase, pyrenes disturb the ordered membrane rather substantially and give rise to a decrease in membrane thickness. This is in agreement with the above-discussed results for the average area per lipid and the S_{CD} order parameters, implying that in the gel phase free pyrenes disturb the local packing of lipids and give rise to local disorder. Above T_M, however, pyrenes lead to a slight increase in membrane thickness, reflecting a minor enhancement of lipid acyl chain ordering. Similar conclusions can be drawn from the mass density profiles, though the effects are then somewhat weaker.

For comparison, electron density profile experiments conducted in the gel phase have given 4.24 nm at 293 K.[58] In the liquid-disordered phase, one has found 3.64 nm at 323 K.[58] Hence, our simulation results are in good agreement with experiments and demonstrate the significant influence of temperature on membrane profiles. Comparison of the details of the mass density profiles indicates that the results for pure DPPC at 325 K are in agreement with previous simulation studies.[35,49,59,60] The shift of P and N distributions in Figure 4 is caused by the expansion of the membrane.

Due to the hydrophobic character of pyrene, we expected it to lie in the hydrophobic core region of the membrane, perhaps even in the membrane center. Experiments by Podo and Blasie for DPPC vesicles[61] and Leonard-Latour et al. for lipid monolayers[62] have also proposed pyrene to be located in the hydrophobic core region. Figure 4 now clearly shows pyrene probes to favor the acyl chain region of DPPC molecules. This preference is most evident in the gel phase, in which case the pyrenes are strongly distributed around $z = 1.0$ nm, that is, in the middle of the acyl chains. The overlap of pyrene and water distributions in the gel phase is almost negligible. In the fluid phase, a small fraction of pyrenes are also occasionally located in the membrane center, though again there is a major and rather broad peak at $z \approx 1.0$ nm, corresponding to carbons 3−8 in the acyl chains; see Figure 5. Thus, pyrenes in the fluid phase prefer to position themselves quite near the glycerol region of the bilayer. These results are in good agreement with previous simulation studies of pyrene in a lipid membrane[20] and with experimental measurements where pyrenes were mostly found between carbons C5 and C6.[26] The fact that pyrenes reside in the acyl chain region instead of the membrane center implies that intermolecular forces are playing a more important role than entropy. This is also evident from the temperature dependence, as the mass density profiles of pyrene become broader and more concentrated in the membrane center at higher temperatures.

Our next goal is to determine the orientation of the probe. Figure 6A and C shows the dependence of the orientation of pyrene on its location in a membrane. The location was characterized by the center-of-mass position of pyrene in the membrane normal direction and the orientation of pyrene by θ, which is the angle between the plane of the flat side of pyrene and the plane of the membrane (in practice determined by the normal of the pyrene plane with respect to the membrane normal direction). In the gel phase (Figure 6A and B), we again find that pyrenes are characterized by a narrow distribution around $z = 1.0$ nm, whereas, in the fluid phase, the distribution is more diffuse (Figure 6C and D). The distribution of pyrene orientations is broader, however. Figure 6A and C shows that the angles, θ, range between 20 and 160° for both phases. Thus, pyrenes do not prefer orientations where they are in parallel with the plane of the membrane. Instead, orientations with larger angles are more likely. Figure 6B and D depicts this in more detail through histograms where the z-dependence of the orientation probability plots is averaged. In the case of the fluid phase depicted in Figure 6D, the events are largely symmetric with respect to 90° for each pyrene in a membrane. This angle corresponds to an orientation where the pyrene is standing upright along the acyl chains. Hoff et al.[20] have found largely similar behavior. In the gel phase, however, the histogram in Figure 6B has two maxima around 50 and 90°. This spread is in part due to insufficient statistics in the gel phase, where the dynamics is very slow. However, another and more important reason for the deviation from 90° is the tilt of acyl chains in the gel phase. The pyrenes try to accommodate themselves in the acyl chain region, where the average tilt of hydrocarbon chains with respect to the membrane normal is about 33°. This in turn affects pyrene orientations. The reason why the second peak is not precisely around 60° is likely due to the local perturbations in lipid packing induced by the probe. Nonetheless, there is reason to stress that the results for pyrene orientations in the gel phase should be considered as suggestive, since the slow dynamics inevitably plays a role here. A thorough description of pyrene conformational states in the gel phase would require simulations of the order of microseconds, which currently is not feasible.

Finally, we also computed the order parameter of the pyrene with respect to the membrane normal. The reason why this topic is interesting is due to the fact that hydrophobic fluorescent probes are rather commonly used to gauge information of membrane fluidity. Then, one assumes that the orientational ordering of the probe reflects the conformational ordering of lipid acyl chains, the latter being characterized by the S_{CD} order parameter. To consider this topic for pyrene, we used the same approach as in S_{CD} but now considering the angle between the membrane normal and the principal axis given by the 1−8 vector in pyrene; see Figure 2b. Using this idea, we compute the average order parameter of pyrene, S_{pyr}. Though it cannot be compared quantitatively with S_{CD}, it allows one to qualitatively assess the coupling between the ordering of pyrene and lipid acyl chains.

The average order parameter values, S_{pyr}, were found to be 0.15 ± 0.06 at 273 K, 0.27 ± 0.05 at 325 K, and 0.19 ± 0.02 at 350 K. The result at 325 K is in agreement with the results

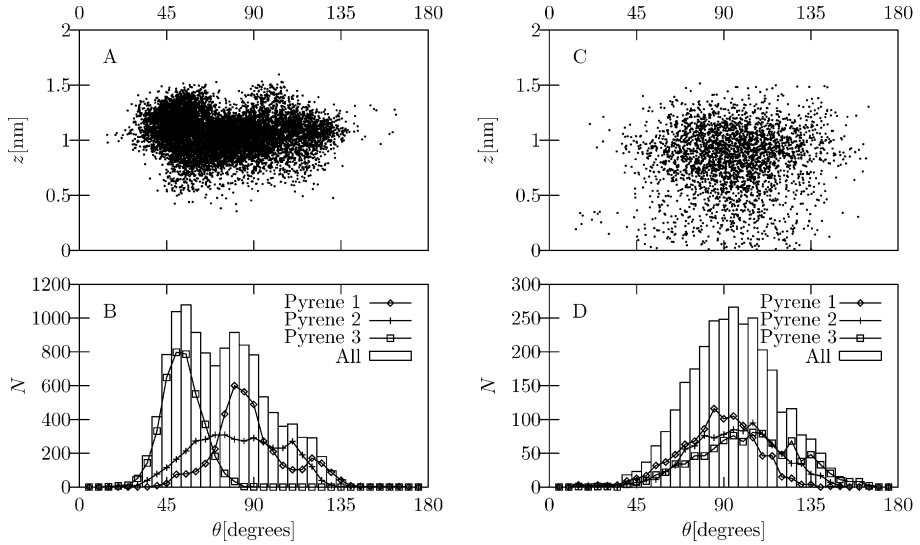

Figure 6. Probability distribution plots of pyrene orientation with respect to the center-of-mass position of the pyrene probe. The orientation is described by the tilt angle, θ, which is defined as an angle between the plane of a flat pyrene moiety and the *xy*-plane of the membrane. Results are shown for (A) the gel phase at 273 K and (C) the liquid-disordered phase at 325 K, determined from simulations where three pyrenes are embedded in the bilayer. Further, we show data for a histogram of pyrene orientations averaged over the *z* positions in the (B) gel and (D) liquid-disordered phases. In all cases, the case $z = 0$ corresponds to the center of the lipid bilayer, $\theta = 0°$ means that the normal of the pyrene plane is in parallel to the membrane normal, and $\theta = 90°$ means that the normal of the pyrene plane is perpendicular to the membrane normal direction.

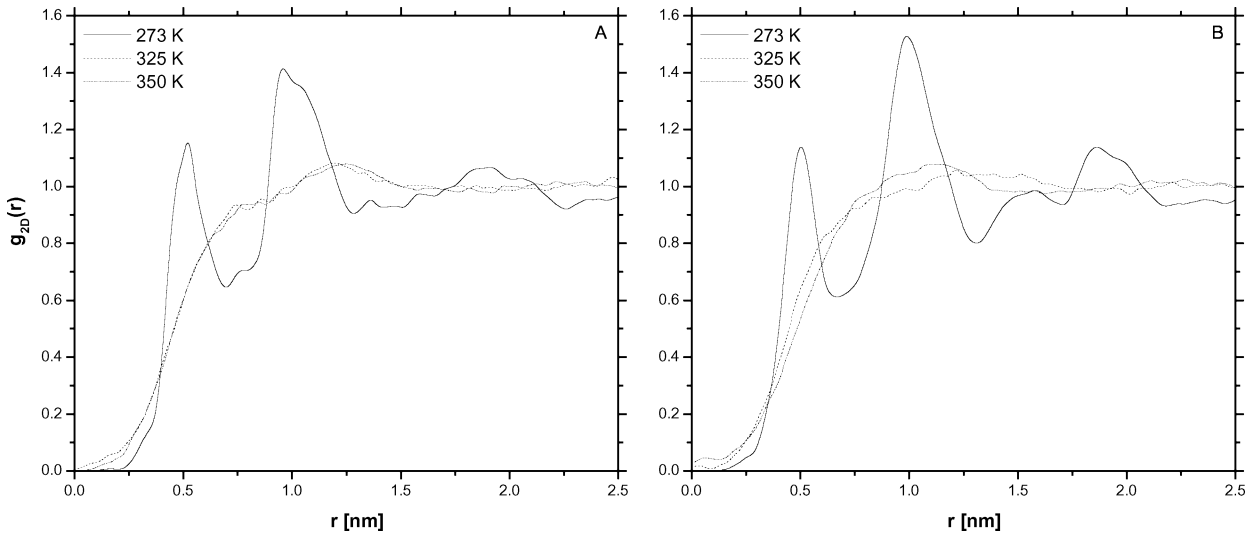

Figure 7. Radial distribution function, $g_{2D}(r)$, for the center-of-mass positions of DPPC molecules at different temperatures in the bilayer plane. Results are shown for systems (A) without pyrene and (B) with three pyrenes.

of Hoff et al.,[20] who found a value of 0.33 at 300 K. The result by Hoff et al. is for POPC at a lower temperature under conditions where the lipids are more tightly packed, $\langle A \rangle \approx 0.56$ nm^2, which explains the minor difference compared with our result. What is more interesting, though, is the temperature dependence of S_{pyr}. When the results for pyrene are compared with the S_{CD} order parameters for lipid acyl chains (see Figure 3), we find notable differences which actually are *qualitative*. While for lipids S_{CD} decreases monotonously for increasing temperature, for pyrene we find non-monotonic behavior: S_{pyr} at 273 K (gel phase) is considerably smaller than that at 325 K (fluid phase). Further, while for lipids the S_{CD} order parameters change only weakly (∼10%) above T_M, for pyrene the decrease in S_{pyr} is prominent (∼40%).

The results for S_{pyr} are consistent with the above distributions of pyrene orientations shown in Figure 6 and indicate that pyrene orientations are subject to rather strong, temperature-dependent fluctuations. Most importantly, the data express a view that S_{pyr} is not a particularly good measure of lipid acyl chain ordering. While it provides the correct qualitative behavior in the fluid phase, its capability to predict the correct temperature dependence is limited.

D. Radial Distribution Functions. To characterize phase behavior, we considered radial distribution functions (RDFs) which describe the radial probability distribution of particles with respect to a uniformly distributed system. Changes in phase behavior should explicitly be observed in the RDF.

We calculated RDFs for the center-of-mass positions of DPPC molecules; see Figure 7. The RDFs at temperatures of 325 and 350 K are consistent with the fluidlike phase with a small peak around 1.2 nm, followed by rapid decay to one with no further density correlations. In the gel phase at 273 K, we find several noticeable peaks whose peak heights decrease at long distances. This is characteristic to the quasi-long-range order often observed, for example, in liquid crystals. Here, we find that the correlations in the RDF at 273 K level off at a correlation distance of about 2.0−2.5 nm. This indicates that, despite the strongly packed nature of the gel phase, there is reasonable free

TABLE 4: Lateral Diffusion Coefficient of DPPC at Different Temperatures and Pyrene Concentrations

temp (K)	pyrene/lipid ratio 0:128	1:128	3:128
273	0.46×10^{-8} cm^2/s	0.38×10^{-8} cm^2/s	0.32×10^{-8} cm^2/s
325	14.67×10^{-8} cm^2/s	14.85×10^{-8} cm^2/s	15.22×10^{-8} cm^2/s
350	43.62×10^{-8} cm^2/s	48.78×10^{-8} cm^2/s	44.68×10^{-8} cm^2/s

volume around the lipids, facilitating their slow (local) motion in the bilayer plane, which in turn washes out the density correlations at long distances. At the same time, Figure 7 shows that the influence of pyrene on the radial distribution functions is minor.

Excimer formation is usually observed for concentrations higher than 1:120.[24] In the highest concentration studied in this work, we computed RDFs between the central atoms C15 and C16 of different pyrene molecules (see Figure 2) (data not shown). However, due to the too short time scale of our simulations, clustering of pyrene probes was not observed.

E. Lateral Diffusion. Fluorescent probes are commonly used to measure lateral diffusion. As probes inevitably perturb the membrane matrix, one may wonder whether they also affect the diffusion behavior. To address this possibility, we computed the lateral diffusion coefficient, D_L, by means of Einstein's equation

$$D_L = \lim_{t\to\infty} \frac{\langle[\vec{r}(t)]^2\rangle}{4t} \tag{4}$$

where $\langle[\vec{r}(t)]^2\rangle$ is the mean-squared displacement (MSD) of the CM position of a tagged lipid. Since the CM position of a bilayer fluctuates in time, we have calculated the MSD for DPPCs with respect to the CM position of the corresponding monolayer.[63] The results were further averaged over all time origins and all molecules in the bilayer.

Table 4 shows that the lateral diffusion coefficient increases rather significantly with temperature. The increase is particularly prominent across the gel−fluid boundary. This is in agreement with experimental findings. In the gel phase, the diffusion rate for DPPC has been found to be of the order of 10^{-10} cm^2/s,[64] while, in the fluid phase, experiments typically end up with lateral diffusion coefficients of about 10^{-7} cm^2/s. For example, in pure DPPC bilayers in the fluid phase, fluorescence recovery after photobleaching has given 12.5×10^{-8} cm^2/s[65] at 325 K, and quasi-elastic neutron scattering studies at 333 K have resulted in a lateral diffusion coefficient of 15×10^{-8} cm^2/s.[66] The rather large difference found in the gel phase between the simulation and experimental data is not a surprise. The time scale for a molecule to move over its own size $\ell \approx 0.7$ nm in the bilayer plane is roughly $\ell^2/4D_L \approx 10$ μs in the gel phase. As the simulation time scale is much shorter, it is obvious that simulations probe the short-time behavior instead of the long-time limit, thus giving too large of an estimate for the lateral diffusion coefficient.

If we consider the effective diffusion barrier through the Arrhenius description, we find 40 kJ/mol above T_M. Considering that the force field used in the present model has not been optimized to account for temperature dependence, this result is reasonably close to the value of 31 kJ/mol found for DMPC by NMR.[67] Due to the small number of pyrene molecules, the poor statistics did not allow reliable determination of D_L for free pyrene.

Intriguingly, however, the effect of pyrene concentration on the lateral diffusion is very weak. In all cases we have studied, the lateral diffusion coefficients for DPPCs in pyrene-containing membranes are, on average and within error bounds, equally large compared with the diffusion coefficients in pure DPPC bilayers. When used with small concentrations, free pyrenes seem not to interfere with the (average) lateral dynamics of lipid molecules.

F. Perspective to Gel Formation at 293 K. In addition to the above-discussed cases, we characterized the same systems at 293 K. This temperature is below the main transition temperature of 314 K, yet the simulations were initiated from a fluidlike state, since our objective was to consider the freezing of the bilayer. However, it soon became apparent that the bilayers did not evolve to the true gel phase but instead showed a partly ordered gel-like bilayer with remnants of the fluid phase. This behavior is in accord with recent findings by Marrink et al.[68] for a coarse-grained model of a lipid bilayer. They concluded that the freezing of the bilayer after a temperature quench from the fluid to the gel phase occurred over a time scale of the order of microseconds. Our results are in agreement with this finding. We found the average area per lipid to decrease and the S_{CD} order parameter to increase compared with the results at 325 K, but the results were still largely reminiscent of the fluid phase rather than the gel phase. Small domains of tilted lipids could be observed, but they were in minority with respect to the rest of the system, and the time scale of gel phase formation was obviously large. Further, as the main transition is expected to be of first order and characterized by hysteresis during heating or cooling across the transition temperature, the precise transition temperature for a simulated system of small size is not known a priori. Summarizing, the present findings indicate that observing the spontaneous formation of gel phase structures through atomistic MD simulations is currently not particularly feasible.

G. Perspective to Details in the Force Field. Using the present model (force field) for the single-component DPPC bilayer, we found an average area per lipid of 0.69 nm^2 in the fluid phase and 0.51 nm^2 in the gel phase. These values are somewhat larger than recent experimental estimates (0.48 nm^2 at 293 K and 0.64 nm^2 at 323 K),[51] though the scatter between different experimental studies seems to be rather substantial. Nonetheless, to confirm that our results and conclusions are on a solid ground, we extended the above-discussed simulations by 20 ns using a model where the truncation distance of van der Waals interactions was $r_c = 1.0$ nm instead of 0.9 nm. No further changes were made to the force field. The increase in the truncation distance is expected to enhance the impact of attractive van der Waals interactions, thus slightly decreasing the area per lipid.[40] The additional simulations carried out at 273 and 325 K confirmed this, as they resulted in values of $\langle A\rangle = 0.504$ nm^2 in the gel phase and 0.661 nm^2 in the fluid phase. These results are closer to experimental findings and essentially consistent with them. As for other quantities, the slight change in the force field was found to have only a minor influence on the results. In the single-component DPPC bilayer, the membrane thickness changed from 4.08 to 4.02 nm at 273 K and from 3.38 to 3.42 nm at 325 K upon increasing r_c from 0.9 to 1.0 nm. In a similar manner for the DPPC bilayer which included three pyrene probes, the membrane thickness changed from 3.76 to 3.82 nm at 273 K and from 3.50 to 3.52 nm at 325 K. Further studies of lipid tilts and S_{CD} profiles confirmed that the related changes were also minor and did not change any of the conclusions drawn above.

IV. Concluding Remarks

Fluorescent probes are widely used to explore the structure and dynamics of cellular and model membranes. However,

despite extensive experimental use, their properties and influence on membrane behavior are not well understood. Here, we have complemented previous computational studies of fluorescent probes.[14,18,20] As for pyrene, there is also one previous simulation study which focused on pyrene properties in the fluid phase.[20] In this work, we have focused on pyrene-induced perturbations in the fluid as well as gel phases by considering the effects of free pyrene probes on structural and also, in part, dynamical properties of lipid bilayers.

In both phases, pyrene was found to reside in the hydrophobic part of the lipid bilayer, under the lipid head groups and close to carbons C5 and C6 of lipid hydrocarbon chains (see Figure 1). The orientations of pyrenes somewhat depend on the phase of the membrane. In the fluid phase, pyrenes prefer to stand upright in parallel to the membrane normal direction. For the same reason, as pyrenes are rigid molecules, they *increase* the ordering of lipid hydrocarbon chains in the fluid phase, though the effect is local and extends over 1−2 molecular diameters in the membrane plane only. In the gel phase, we found that the orientations of pyrenes are peaked around two maxima, the first one being as in the fluid phase and the second one corresponding to a slanted alignment due to tilted acyl chains in the gel phase. In this gel case, pyrene locally *decreased* the conformational ordering of nearby lipid chains, reduced the amount of trans states along the acyl chains, and perturbed the packing of lipids, hence slightly increasing the average area per lipid and decreasing the membrane thickess. When it comes to dynamic properties such as the rate of DPPC lateral diffusion, we found only a minor influence due to pyrene.

Overall, our results are in favor of an idea that free pyrene affects membrane properties, but the effects are of local nature and do not significantly affect those lipid properties that are computed over the whole system, such as density profiles. The only exception found here seems to be the membrane thickness in the gel phase, which for reasonable pyrene concentrations decreased by about 7% compared with the pure DPPC bilayer.

As hydrophobic fluorescent probes are rather often used to gather information of membrane fluidity, we also determined the orientational order parameter of pyrene with respect to the membrane normal and compared the results with those found for lipid acyl chains. The data express a view that the orientational ordering of pyrene is not a particularly good measure to describe the ordering of lipid acyl chains. The present work seems to indicate that pyrene provides the correct qualitative behavior for acyl chain ordering in the fluid phase, but its capability to predict the correct temperature dependence is limited, in particular across the gel−fluid transition.

Summarizing, what is perhaps most interesting is the different nature of pyrene-induced perturbations in the gel and fluid phases. In the gel phase, our results indicate that pyrene locally breaks the translational order and decreases the conformational ordering of nearby acyl chains, while, in the fluid phase, pyrene enhances the conformational ordering of lipid acyl chains and hence facilitates better (local) packing of the lipids. One is tempted to think that in this respect pyrene acts like cholesterol, which also breaks the order in the gel phase and increases the local order in the fluid phase. As cholesterol is also a rather small and rigid molecule residing largely in a similar manner as pyrene inside the membrane, this similarity in the effects of the two molecules on membrane properties seems to be largely justified. It would be tempting to study whether this behavior is generic and holds to a large degree for many hydrophobic fluorescent probes embedded inside the membrane.

Acknowledgment. This work is a part of the research plan MSM 0021620835 financed by the Ministry of Education of the Czech Republic and partly supported by FRVS grant 829/2006. Further funding from the Academy of Finland is also acknowledged (Project No. 80246 and the Center of Excellence program).

References and Notes

(1) Gennis, R. B. *Biomembranes: Molecular Structure and Function*; Springer-Verlag: New York, 1989.
(2) Simons, K.; Ikonen, E. *Nature* **1997**, *387*, 569−571.
(3) Mayor, S.; Rao, M. *Traffic* **2004**, *5*, 231−240.
(4) Hancock, J. F. *Nat. Rev. Mol. Cell Biol.* **2006**, *7*, 456−462.
(5) Langer, R. *Nature* **1998**, *392* (Suppl. 6679), 5−10.
(6) Mouritsen, O. G.; Andresen, T. L.; Halperin, A.; Hansen, P. L.; Jakobsen, A. F.; Jensen, U. B.; Jensen, M. O.; Jorgensen, K.; Kaasgaard, T.; Leidy, C.; Simonsen, A. C.; Peters, G. H.; Weiss, M. *J. Phys.: Condens. Matter* **2006**, *18*, S1293−S1304.
(7) Lakowicz, J. R. *Principles of Fluorescence Spectroscopy*; Plenum: New York, 1983.
(8) Schmidt, T.; Schütz, G. J.; Baumgartner, W.; Gruber, H. J.; Schindler, H. *Proc. Natl. Acad. Sci. U.S.A.* **1996**, *93*, 2926−2929.
(9) Lentz, B. R. *Chem. Phys. Lipids* **1993**, *64*, 99−116.
(10) Maier, O.; Oberle, V.; Hoekstra, D. *Chem. Phys. Lipids* **2002**, *116*, 3−18.
(11) Fidorra, M.; Duelund, L.; Leidy, C.; Simonsen, A. C.; Bagatolli, L. A. *Biophys. J.* **2006**, *90*, 4437−4451.
(12) Martins, J.; Melo, E. *Biophys. J.* **2001**, *80*, 832−840.
(13) Holopainen, J. M.; Subramanian, M.; Kinnunen, P. K. J. *Biochemistry* **1998**, *37*, 17562−17570.
(14) Repakova, J.; Capkova, P.; Holopainen, J. M.; Vattulainen, I. *J. Phys. Chem. B* **2004**, *108*, 13438−13448.
(15) Lentz, B. R.; Freire, E.; Biltonen, R. L. *Biochemistry* **1978**, *17*, 4475−4480.
(16) Lentz, B. R. *Chem. Phys. Lipids* **1989**, *50*, 171−190.
(17) Parente, R. A.; Lentz, B. R. *Biochemistry* **1985**, *24*, 6178−6185.
(18) Repakova, J.; Holopainen, J. M.; Morrow, M. R.; McDonald, M. C.; Capkova, P.; Vattulainen, I. *Biophys. J.* **2005**, *88*, 3398−3410.
(19) Repakova, J.; Holopainen, J. M.; Karttunen, M.; Vattulainen, I. *J. Phys. Chem. B* **2006**, *110*, 15403−15410.
(20) Hoff, B.; Strandberg, E.; Ulrich, A. S.; Tieleman, D. P.; Posten, C. *Biophys. J.* **2005**, *88*, 1818−1827.
(21) Somerharju, P. *Chem. Phys. Lipids* **2002**, *116*, 57−74.
(22) Vekshin, N. L. *Anal. Chim. Acta* **1989**, *227*, 267−272.
(23) Baumgart, T.; Hess, S. T.; Webb, W. W. *Nature* **2003**, *425*, 821−824.
(24) Daems, D.; van den Zegel, M.; Boens, N.; de Schryver, F. C. *Eur. Biophys. J.* **1985**, *12*, 97−105.
(25) Castelli, F.; Librando, V.; Sarpietro, M. G. *Thermochim. Acta* **2001**, *373*, 133−140.
(26) Herrenbauer, M. *Biosorption von Polyzyklischen Aromatischen Kohlenwasserstoffen (PAK) an Mikroorganismen und Liposomen.*; Shaker Verlag: Aachen, Germany, 2000.
(27) Venable, R. M.; Brooks, B. R.; Pastor, R. W. *J. Chem. Phys.* **2000**, *112*, 4822−4832.
(28) Essman, U.; Perera, L.; Berkowitz, M. L. *Langmuir* **1995**, *11*, 4519−4531.
(29) Tu, K.; Tobias, D. J.; Blasie, J. K.; Klein, M. L. *Biophys. J.* **1996**, *70*, 595−608.
(30) Heller, H.; Schaefer, M.; Schulten, K. *J. Phys. Chem.* **1993**, *97*, 8343−8360.
(31) Sum, A. K.; Faller, R.; de Pablo, J. J. *Biophys. J.* **2003**, *85*, 2830−2844.
(32) Tristram-Nagle, S.; Zhang, R.; Suter, R. M.; Worthington, C. R.; Sun, W. J.; Nagle, J. F. *Biophys. J.* **1993**, *64*, 1097−1109.
(33) Tristram-Nagle, S.; Zhang, R.; Suter, R. M.; Worthington, C. R.; Sun, W.-J.; Nagle, J. F. *Biophys. J.* **1993**, *64*, 1097−1109.
(34) Repakova, J.; Holopainen, J. M.; Karttunen, M.; Vattulainen, I. Manuscript in preparation, 2006.
(35) Tieleman, D. P.; Berendsen, H. J. C. *J. Chem. Phys.* **1996**, *105*, 4871−4880.
(36) *Cerius*^{2} *property prediction*; Molecular Simulations Inc.: San Diego, CA, 1997.
(37) Berger, O.; Edholm, O.; Jahnig, F. *Biophys. J.* **1997**, *72*, 2002−2013.
(38) Frisch, M. J.; Trucks, G. W.; Schlegel, H. B.; Scuseria, G. E.; Robb, M. A.; Cheeseman, J. R.; Zakrzewski, V. G.; Montgomery, J. A., Jr.; Stratmann, R. E.; Burant, J. C.; Dapprich, S.; Millam, J. M.; Daniels, A. D.; Kudin, K. N.; Strain, M. C.; Farkas, O.; Tomasi, J.; Barone, V.; Cossi, M.; Cammi, R.; Mennucci, B.; Pomelli, C.; Adamo, C.; Clifford, S.;

Ochterski, J.; Petersson, G. A.; Ayala, P. Y.; Cui, Q.; Morokuma, K.; Malick, D. K.; Rabuck, A. D.; Raghavachari, K.; Foresman, J. B.; Cioslowski, J.; Ortiz, J. V.; Stefanov, B. B.; Liu, G.; Liashenko, A.; Piskorz, P.; Komaromi, I.; Gomperts, R.; Martin, R. L.; Fox, D. J.; Keith, T.; Al-Laham, M. A.; Peng, C. Y.; Nanayakkara, A.; Gonzalez, C.; Challacombe, M.; Gill, P. M. W.; Johnson, B. G.; Chen, W.; Wong, M. W.; Andres, J. L.; Head-Gordon, M.; Replogle, E. S.; Pople, J. A. *Gaussian 98*; Gaussian, Inc.: Pittsburgh, PA, 1998.

(39) Berendsen, H. J. C.; Postma, J. P. N.; Gunsteren, W. F.; Hermans, J. *Intermolecular Forces*; Reidel: Dordrecht, The Netherlands, 1981.

(40) Patra, M.; Karttunen, M.; Hyvnen, M. T.; Falck, E.; Lindqvist, P.; Vattulainen, I. *Biophys. J.* **2003**, *84*, 3636−3645.

(41) Patra, M.; Karttunen, M.; Hyvnen, M. T.; Falck, E.; Vattulainen, I. *J. Phys. Chem. B* **2004**, *108*, 4485−4494.

(42) Essman, U.; Perera, L.; Berkowitz, M. L.; Darden, T.; Lee, H.; Pedersen, L. G. *J. Chem. Phys.* **1995**, *103*, 8577−8593.

(43) Patra, M.; Hyvonen, M.; Falck, E.; Sabouri-Ghomi, M.; Vattulainen, I.; Karttunen, M. *Comput. Phys. Commun.* **2007**, *176*, 14−22.

(44) Lindahl, E.; Hess, B.; van der Spoel, D. *J. Mol. Model.* **2001**, *7*, 306−317.

(45) Hess, B.; Bekker, H.; Berendsen, H. J. C.; Fraaije, J. G. E. M. *J. Comput. Chem.* **1997**, *18*, 1463−1472.

(46) Gurtovenko, A. A.; Vattulainen, I. *J. Am. Chem. Soc.* **2005**, *127*, 17570−17571.

(47) Kupiainen, M.; Falck, E.; Ollila, S.; Niemela, P.; Gurtovenko, A. A.; Hyvonen, M. T.; Patra, M.; Karttunen, M.; Vattulainen, I. *J. Comput. Theor. Nanosci.* **2005**, *2*, 401−413.

(48) Falck, E.; Patra, M.; Karttunen, M.; Hyvnen, M. T.; Vattulainen, I. *J. Chem. Phys.* **2004**, *121*, 12676−12689.

(49) Falck, E.; Patra, M.; Karttunen, M.; Hyvonen, M. T.; Vattulainen, I. *Biophys. J.* **2004**, *87*, 1076−1091.

(50) Vainio, S.; Jansen, M.; Koivusalo, M.; Rog, T.; Karttunen, M.; Vattulainen, I.; Ikonen, E. *J. Biol. Chem.* **2006**, *281*, 348−355.

(51) Nagle, J. F.; Tristam-Nagle, S. *Biochim. Biophys. Acta* **2000**, *1469*, 159−195.

(52) Seelig, A.; Seelig, J. *Biochemistry* **1974**, *13*, 4839−4845.

(53) Tieleman, D. P.; Marrink, S. J.; Berendsen, H. J. *Biochim. Biophys. Acta* **1997**, *1331*, 235−270.

(54) Egberts, E.; Berendsen, H. J. C. *J. Chem. Phys.* **1988**, *89*, 3718−3732.

(55) Petrache, H. I.; Dodd, S. W.; Brown, M. F. *Biophys. J.* **2000**, *79*, 3172−3192.

(56) Tu, K.; Klein, M. L.; Tobias, D. J. *Biophys. J.* **1998**, *75*, 2147−2156.

(57) Sum, W.-J.; Suter, R. M.; Knewtson, M. A.; Worthington, C. R.; Tristram-Nagle, S.; Zhang, R.; Nagle, J. F. *Phys. Rev. E* **1994**, *49*, 4665−4676.

(58) Nagle, J. F.; Zhang, R.; Tristram-Nagle, S.; Sun, W.; Petrache, H. I.; Suter, R. M. *Biophys. J.* **1996**, *70*, 1419−1431.

(59) Chiu, S. W.; Jakobsson, E.; Mashl, R. J.; Scott, H. L. *Biophys. J.* **2002**, *83*, 1842−1853.

(60) Hofsass, C.; Lindahl, E.; Edholm, O. *Biophys. J.* **2003**, *84*, 2192−2206.

(61) Podo, F.; Blasie, J. K. *Proc. Natl. Acad. Sci. U.S.A.* **1977**, *74*, 1032−1036.

(62) Leonard-Latour, M.; Morelis, R. M.; Coulet, P. R. *Langmuir* **1996**, *12*, 4797−4802.

(63) Patra, M.; Karttunen, M.; Hyvnen, M. T.; Falck, E.; Vattulainen, I. *J. Phys. Chem. B* **2004**, *108*, 4485−4494.

(64) Ulmius, J.; Wennerström, H.; Lindblom, G.; Arvidson, G. *Biochim. Biophys. Acta* **1975**, *389*, 197−202.

(65) Vaz, W. L.; Clegg, R. M.; Hallmann, D. *Biochemistry* **1985**, *24*, 781−786.

(66) Konig, S.; Pfeiffer, W.; Bayerl, T.; Richter, D.; Sackmann, E. *J. Phys. II* **1992**, *2*, 1589−1615.

(67) Filippov, A.; Oradd, G.; Lindblom, G. *Biophys. J.* **2003**, *84*, 3079−3086.

(68) Marrink, S. J.; Risselada, J.; Mark, A. E. *Chem. Phys. Lipids* **2005**, *135*, 223−244.